Available online at www.sciencedirect.com
SCIENCE DIRECT®
International Journal of Heat and Mass Transfer 48 (2005) 2420–2428
International Journal of HEAT and MASS TRANSFER
www.elsevier.com/locate/ijhmt

Experimental study of impinging heat transfer along rib-roughened walls by using transient liquid crystal technique

W.M. Yan [a,*], H.C. Liu [a], C.Y. Soong [b], W.-J. Yang [c]

[a] Department of Mechatronic Engineering, Huafan University, Shih Ting, Taipei 22305, Taiwan, ROC
[b] Department of Aerospace and System Engineering, Feng Chia University, Seatwen, Taichung 40745, Taiwan, ROC
[c] Department of Mechanical Engineering and Applied Mechanics, University of Michigan, Ann Arbor, MI 48109-2125, USA

Received 3 May 2004; received in revised form 31 December 2004
Available online 26 March 2005

Abstract

The objective of this work is to examine the detailed heat transfer coefficient distributions over a ribbed surface under impingement of in-line and staggered jet arrays by using a liquid crystal thermograph technique. In-line and staggered jet arrays with different exit flow orientations were considered. Three jet-to-target spacing Z of 3, 6 and 9 with in-line and staggered jet arrays were considered at jet Reynolds numbers of Re = 1500, 3000 and 4500 with three different exit flow orientations. In addition, the effects of rib configuration on the heat transfer distributions were discussed in detail. Results show that the local heat transfer rates over the ribbed surface are characterized by obvious periodic-type variation of Nusselt number distributions. The downstream peaks are diminished for increasing cross flow effect. Compared to the results without ribs, the heat transfer over the ribbed surface may be enhanced or retarded. Whereas, among the test angled-rib arrangements, the best heat transfer performance is obtained with a surface with 45° angled ribs.

1. Introduction

Jet impingement and ribbed surface are both effective means for heat transfer enhancement and have been used in a variety of practical applications, e.g. cooling of hot steel plate, gas turbine cooling, thermal management of microelectronic components, etc. In the past decades, the effects of various parameters on the flow field and heat transfer characteristics under an impinging jet array of air and liquid have been explored extensively [1,2]. Most of the studies concentrated on the high transport rates caused by impingement and the heat transfer degradation by the cross flow effect.

For heat transfer associated with an array of impinging jets, the effects of the jet array pattern, Reynolds number, cross flow, jet-to-target distance and their coupling effects significantly influence the flow and heat transfer characteristics. There exists a considerable body of literature to deal with the fluid flow and heat transfer characteristics under an array of air impinging jets [1,3]. In recent years, many investigators [2,4] have been explored heat transfer characteristics of an array of liquid impinging jets. They focused largely on the heat transfer under impinging jets for which cross flow effects, which potentially degrade the high stagnation heat transfer associated with impinging jets, are designed to be minimal.

* Corresponding author. Tel.: +886 2 2663 2102; fax: +886 2 2663 1119.
E-mail address: wmyan@huafan.hfu.edu.tw (W.M. Yan).

0017-9310/$ - see front matter © 2005 Elsevier Ltd. All rights reserved.
doi:10.1016/j.ijheatmasstransfer.2004.12.048

Nomenclature

d	diameter of impinging jet port
h	local heat transfer coefficient, W/m^2 K
k	thermal conductivity of acrylic material, W/m K
k_f	air thermal conductivity, W/m K
Nu	Nusselt number, hd/k_f
Re	jet Reynolds number, Vd/v
T_i	initial temperature of the target surface, °C or K
T_∞	mainstream temperature of the air flow, °C or K
T_w	color change temperature of the liquid crystal, red-to-green, °C or K
t	transient test time, s
V	average velocity of impinging jet, m/s
X, x	dimensionless and dimensional axial distance of the target surface, $X = x/d$
Y, y	dimensionless and dimensional spanwise distance, $Y = y/d$
Z, z	dimensionless and dimensional spacing between jet plate and target plate, $Z = z/d$
Greek symbols	
α	thermal diffusivity of acrylic material, m^2/s
γ	dimensionless time variable defined in Eq. (2), $h\sqrt{\alpha t}/k$
v	kinematic viscosity of air, m^2/s
τ_j	time step, s

Recently, thermochromic liquid crystal (TLC) has been used as a reliable temperature sensor to measure heat transfer coefficients. The liquid crystal thermograph has become a widely-used technique for its merits of whole surface heat transfer measurements. Detailed heat transfer distributions under arrays of jets impinging on a target plate with dimpled or film hole surfaces were investigated by Treuren et al. [5], Huang et al. [6] and Azad et al. [7] disclosed that the cross flow and the exit flow direction significantly affect the heat transfer distributions on a target surface. Their results concerned on heat transfer under in-line arrays of jets impinging on a surface with only one fixed jet-to-plate spacing. Recently, also by using transient TLC techniques, we accomplished a study on heat transfer enhancement over a base plate with obstacles effects [8]. However, the studies in the past are mostly on a flat surface with relatively few over a curved surface [9]. In a practical situation, the surface which needs to be cooled may not be smooth and may be roughened. In order to achieve enhanced heat transfer, periodic ribs are often employed in the design of gas turbine engines and heat exchangers. Gau and Lee [10] performed an experimental study of impinging jet flow structure and heat transfer along the rib-roughened wall. In their study, a single jet flow is considered only. As for the study about rib turbulators on the heat transfer and pressure drop along a channel or a multi-pass channel, Han and his colleagues [11–15] have examined systematically the effects of rib height, rib pitch, rib angle of attack, etc., on the heat transfer.

But from the literature reviews presented above, it is found that the effects of cross flow on the impinging heat transfer along rib-roughened walls are not well examined. The objective of the present work is to study the detailed heat transfer coefficient over rib-roughened walls under in-line or staggered jet array by using a transient liquid crystal technique. The effects of rib configuration on the heat transfer distributions were explored. Three rib configurations, 90° transverse ribs, and 60° and 45° angled ribs, were tested. In addition, the effects of cross flow, exit flow orientation and jet Reynolds number are investigated. To resolve the highly localized heat transfer distributions, a transient liquid crystal technique in connection with a thin film of thermochromic liquid crystal (TLC) coated directly on the impingement target surface is employed to measure the local heat transfer distributions. During a transient test, the color change of TLC film on the target surface was monitored and recorded by an automatic computer vision system and a data acquisition system. The time of color change of the liquid crystal to green[1] is measured using an image processing equipment.

2. Experimental apparatus and procedure

Fig. 1 presents a schematic of the experimental facility which consists of a blower, a small wind tunnel, a computerized data acquisition, image process system and a test section. The test section has two compartments separated by a jet plate having an array of jet ports of diameter $d = 5$ mm. The top compartment is a pressure chamber, while the bottom compartment is the impingement channel, whose bottom is referred to as target plate. On the jet plate, 9 (streamwise) × 5 (spanwise) jet holes are drilled in an in-line or a staggered pattern. The thickness of the jet plate is equal to the jet hole diameter. The port-to-port spacing in the axial direction (x) is six times the hole diameter, while the port-to-port spacing in the spanwise direction (y) is three times the

[1] For interpretation of color in Figs. 4–9, the reader is referred to the web version of this article.

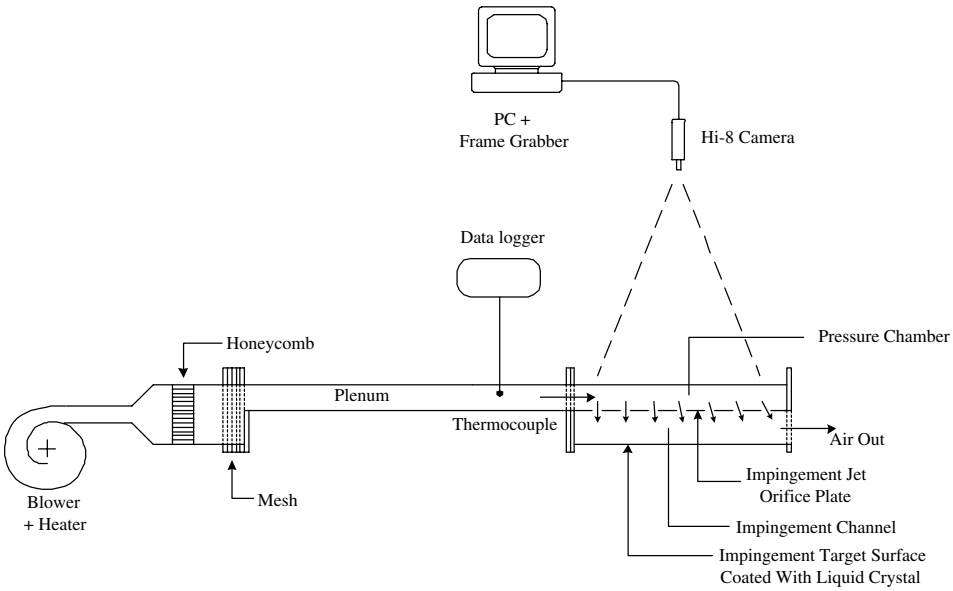

Fig. 1. Schematic diagram of the physical system.

hole diameter. The inlet pressure chamber has a cross section of 100 mm × 50 mm. The target surface with rib arrangement coated with liquid crystal is of 10 mm in thickness and 300 mm × 100 mm in area. The rib pitch, width and height are 30 mm, 5 mm and 2.5 mm, respectively.

The test section is made of clear acrylic material so that the camera can see through. The impingement target surface is made from black acrylic and coated a thin film of TLC on the inside surface. The choice of the black acrylic is due to its low thermal conductivity. The computerized data acquisition system contains a digital image processing system and a data logger. The image processing system used in this work was composed of a digital color camcorder (camera + image recorder, SONY DCR-TRV7), a frame grabber card, and a Pentium IV personal computer. The isotherms of red-to-blue transition band were captured through a digital color camcorder with 682 × 492 pixels resolution. These captured images were digitized by a frame grabber consisting of 260 × 220 pixels with 256 gray levels and then processed by Pentium IV PC.

Since the actual color image can be affected from many factors such as the thickness and surface condition of liquid crystal, the angle of camera and lighting illuminator, a careful temperature calibration of liquid crystal has to be done. The TLC and thermocouples with a FLUKE Helios Plus data logger were used. The liquid crystal was calibrated using the digital image processing system under the same conditions of experimental runs, including the illuminating light and the camera-viewing angle. The detailed test procedure can be found elsewhere [8,16,17].

3. Heat transfer theory

For the acrylic plastic test surface material used, the depth of heating into the plate over the time duration needed to complete the experimental run is less than the target plate thickness. In addition, lateral conduction in the plate is not expected to have a considerable effect on the local surface temperature response. At any surface point, the target plate temperature is thus represented by the classical one-dimensional response of a semi-infinite medium to the sudden step application of a convective fluid at temperature T_∞. The following equation describes the surface temperature.

$$(T_w - T_i)/(T_\infty - T_i) = 1 - \exp(\gamma^2)\mathrm{erf}\, c(\gamma) \quad (1)$$

where

$$\gamma = h\sqrt{\alpha t}/k \quad (2)$$

In the above, T_i is the initial temperature of the test surface and the T_∞ stands for the jet flow temperature. Acrylic properties, thermal diffusivity α and thermal conductivity k, are known. In order to determine the local heat transfer coefficient h, the color change temperature T_w for the coated-surface color being green was determined based on the calibration of liquid crystal change temperature. The corresponding time, t, to reach this temperature for any location on the target surface is measured by using the image processing system. The time required for color change in a typical experimental run is about 15–90 s depending on the locations and conditions of experiment runs.

However, in the actual experiments, the target surface will not experience a step change in the driving air

temperature due to the transient heating of the upstream jet nozzle pieces and duct walls. Nevertheless, Eq. (1) is a fundamental solution that can be used to represent the response to a superposed set of gradual changes in T_∞. Using the Duhamel's superposition theorem, the solution in Eq. (1) is represented as

$$T_w - T_i = \sum_{j=1}^{n} \left\{ 1 - \exp\left[\frac{h^2\alpha(t-\tau_j)}{k^2}\right] \times \operatorname{erf} c\left[\frac{h\sqrt{\alpha(t-\tau_j)}}{k}\right] \right\} [\Delta T_{\infty j}] \quad (3)$$

where ΔT_∞ and τ_j are the temperature and time step changes from the recorder output of the jet flow temperature history. In the present experiments, jet flow temperature T_∞ is determined from thermocouple measurement in the pressure chamber prior to jet issue. The T_∞ variation with time is recorded and approximated by steps, and the resulting superposed solution, Eq. (3), is solved for the local surface heat transfer coefficients, using the color change times t at any location.

4. Results and discussion

Jet impingement heat transfer depends on several flow and geometry parameters, including jet Reynolds number (Re), Prandtl number of jet flow (Pr), jet-to-jet spacing, jet-to-plate spacing (Z), jet array pattern (in-line or staggered), target surface geometry and exit flow direction. In this work, the emphasis is focused on the effects of rib arrangement, jet array pattern (in-line or staggered), and jet-to-target spacing (Z) under different jet Reynolds numbers (Re) and spent -air cross flow orientations. The flow enters the pressure chamber from one end ($X = 0$) and, after being ejected into the impingement channel, the fluid exits the impingement channel. Three types of exit flow denoted as flow orientations 1, 2 and 3 are tested as shown schematically in Fig. 2. The flow orientation 1 means that the flow exits from the other end ($X = 60$), i.e., the flow enters and exits its test section in the same direction. In the case with flow orientation 2, the flow enters the pressure chamber from $X = 0$ and exits the impingement channel from both ends ($X = 0$ and 60). With the flow orientation 3, the flow in the impingement channel exits in the opposite direction of the entry flow in the pressure chamber.

In the three types of exit flows, the global flow rate is provided as one of the governing parameters, but the local flow rate distribution along the channel axis is not controlled artificially. Therefore, it is very interesting as well as significant to understand the variation of the jet velocities from port to port along the longitudinal direction. The longitudinal variation of the spanwise

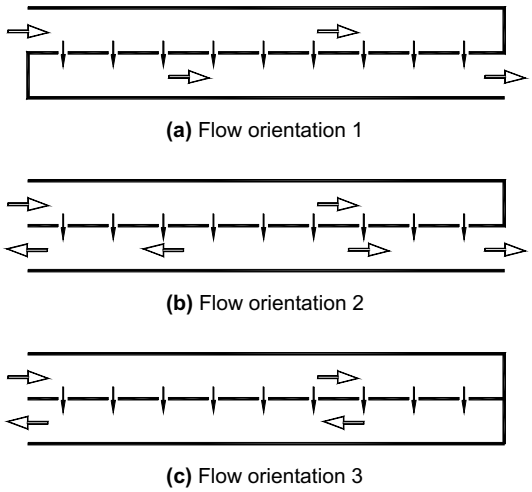

Fig. 2. Schematic diagram of the exit flow orientations.

average of jet velocity and the local mass flow rate accumulated along the X-direction can be found elsewhere [16].

To compare the present results with the existing experimental results, the averaged $\overline{Nu}$ at various conditions are shown in Fig. 3. It is clear that the present data of ribbed wall with 45° rib arrangement show similar trend as the previous results on smooth wall at various values of Z. Comparing the results between the in-line jet impingement on ribbed and smooth walls, it indicates that better heat transfer is noted for jet impingement on ribbed wall. As for the staggered jet impingement, the same trend is also found for $Re = 1500$ and 3000. But for $Re = 4500$, the averaged $\overline{Nu}$ is almost the same for both the in-line and staggered jet impingements. It is worth noting that for the in-line or staggered impingement, the jet impingement on the ribbed wall with 45° angled ribs is always larger than that on the smooth wall for $Z = 6$ and flow orientation 2.

Fig. 4 shows the Nu-contours with ribs of 45° at various exit conditions. For flow orientation 1 in Fig. 4(a), the cross flow is weak in the upstream portion (small X) of the impingement channel. The high-Nu distributions almost align with the jet-hole locations. As the cross flow develops along the X-direction, the locations of the high-Nu spots are significantly shifted downstream. The extent of shift increases with X for the increasing spent-air cross flow effects. For the flow orientation 3 in Fig. 4(c), the flow exits in the opposite direction of the flow entrance. In this case, the cross flow effect is relatively small at a location of large X, where the heat transfer shows better performance than that near the exit. While the cross flow effect shifts in the impingement location toward the exit at $X = 0$. The extent of the shift is more significant near the exit end ($X = 0$) due to the

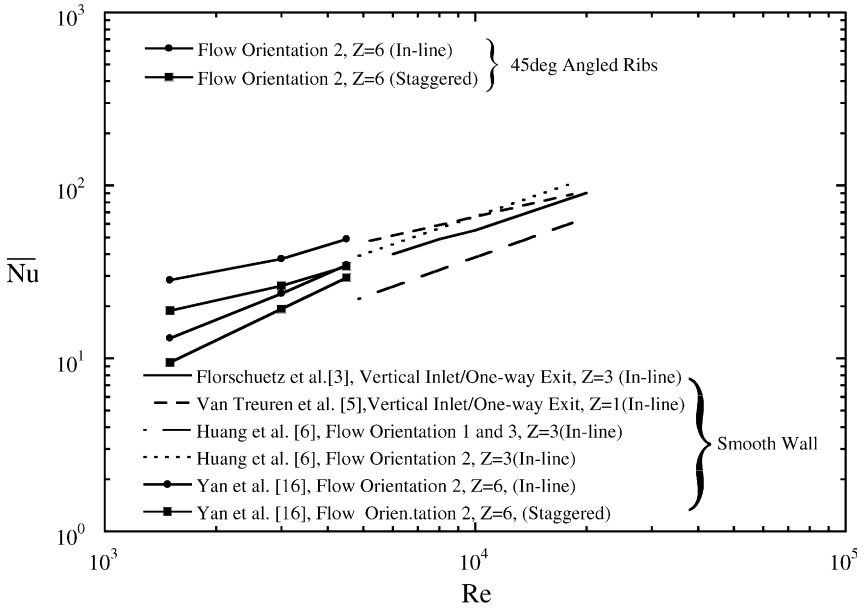

Fig. 3. Comparison of averaged Nusselt number with previous multiple jet correlations.

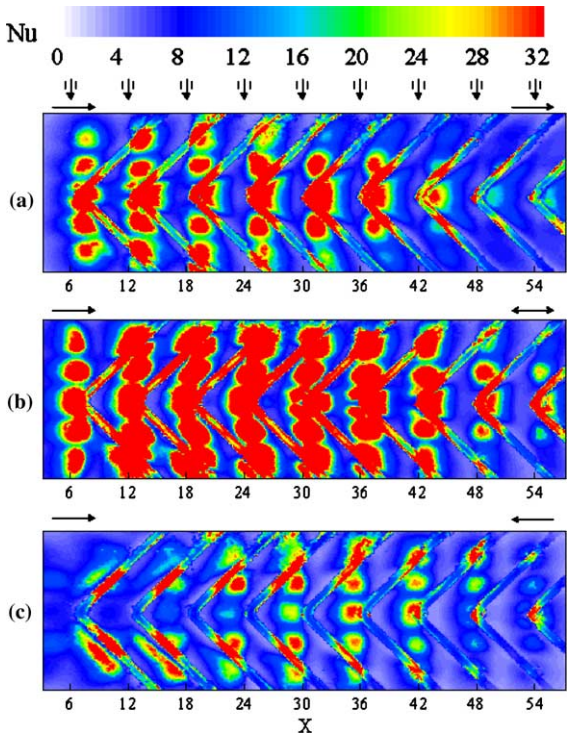

Fig. 4. Effects of flow orientation on local heat transfer distributions for in-line jet array at $Re = 3000$, $Z = 6$, rib angle of 45° and flow orientations (a) 1; (b) 2 and (c) 3.

stronger cross flow effects. Close comparison of the three cases indicates that the heat transfer distributions are strongly affected by the cross flow effects. With the flow orientation 2, see Fig. 4(b), the jet impinging effect performs the highest heat transfer rates among the three exit flow conditions. This can be made plausible by noting the fact that, with orientation 2, all the spent air may exit easily through the both exit ends with no need to go through the whole impingement channel. Therefore, the best heat transfer performance can be obtained at the exit flow condition of both ends open, of which the heat transfer deterioration due to the cross flow effect is minimized.

Fig. 5 presents the results of the effects of flow orientation on the local heat transfer distributions for staggered jet array. By comparing Figs. 4 and 5, it indicates that the effects of the flow orientation on the local Nusselt number are similar for both in-line and staggered jet arrays. But a careful examination of Figs. 4 and 5 discloses that better heat transfer performance is noted for the in-line jet array.

After discussing the effects of flow orientation, the effects of jet Reynolds number Re on the impingement heat transfer are also important in many industrial applications. Fig. 6 presents the effects of jet Reynolds number Re on the detailed heat transfer coefficients for flow orientation 2. In Fig. 6, the subplots (a), (b) and (c) correspond to the cases with $Re = 1500$, 3000 and 4500, respectively. The results show that the local heat transfer coefficient depends on the jet Reynolds number Re and increases with an increase in the jet Reynolds number Re. This confirms the concept that for convective heat transfer, better heat transfer is noted for a case with a higher Reynolds number. Like the results in

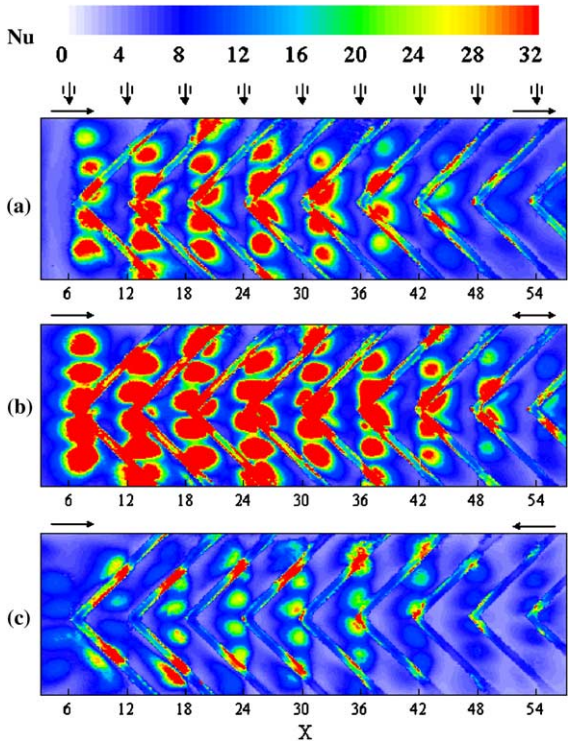

Fig. 5. Effects of flow orientation on local heat transfer distributions for staggered jet array at $Re = 3000$, $Z = 6$, rib angle of 45° and flow orientations (a) 1; (b) 2 and (c) 3.

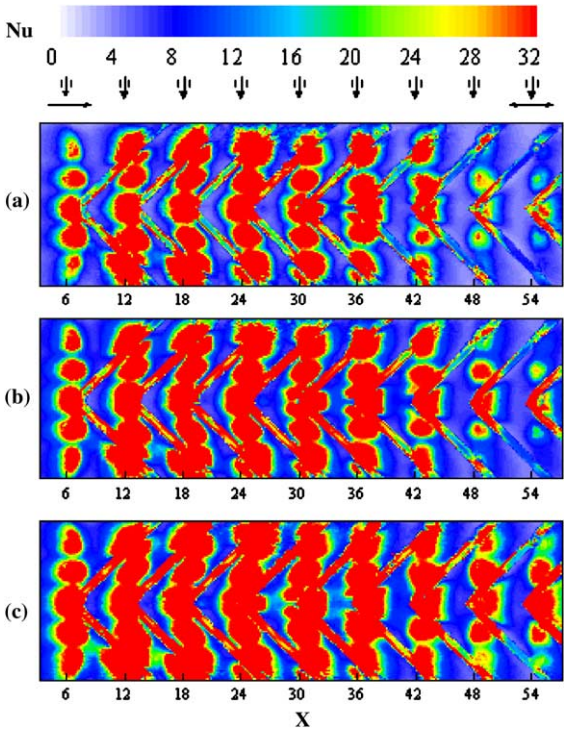

Fig. 6. Effects of Reynolds number on local heat transfer distributions for in-line jet array at $Z = 6$, flow orientation 2, rib angle of 45° and Reynolds Number (a) 1500; (b) 3000 and (c) 4500.

Fig. 4, the local Nusselt numbers decreases as the spent air exits toward both ends ($X = 0$ and 60).

For the study of internal cooling of turbomachinery, the information of jet impingement heat transfer with different jet-to-plate spacing is important to the related designer. Therefore, it is interesting to examine the effects of jet-to-plate spacing Z on the local Nu distributions. Fig. 7 shows the local impinging heat transfer under in-line jet array with different jet-to-plate spacing. As expected, the impinging force on the target surface is stronger for a smaller jet-to-plate spacing Z. Therefore, larger Nu distributions are found for a smaller Z. In addition, it is clearly seen that the shifts of high-Nu spots are relatively significant for a larger Z due to a smaller impinging force. The numerical comparisons of the averaged Nusselt number $\overline{Nu}$ between the in-line and staggered jet arrangements are presented in Table 1. It is clear in Table 1 that for the jet impingement on the smooth wall, the averaged Nusselt number of in-line jet impingement is larger than that of staggered jet arrangement for $Z = 3$ and 6. But, for $Z = 9$, better heat transfer is noted for staggered jet arrangement. As for the heat transfer of the jet impingement on the ribbed wall, the averaged Nusselt number of in-line jet arrangement is always larger than that of staggered jet arrangement for different Z.

To enhance the heat exchange between the fluids and the solid, ribs are usually mounted on the heat transfer surface. But for the inappropriate rib arrangement, the presence of the ribs may retard the flow motion and the heat transfer. Therefore, the geometric arrangement of the ribs can be one of the significant factors. In Fig. 8, with the exit flow orientation 2, presents the rib-angle effects on the local heat transfer distributions under in-line jet array. In the case of 90° rib angle, see Fig. 8(a), the ribs just lie beneath the spanwise row of jet ports and impinged by the jets directly. It is observed in Fig. 8(a) that on the top of the rib the high heat transfer rate occurs. However, the impinging regions characterized by the high heat transfer spots in the Nu-contours shift slightly toward the exits due to the cross flow effects. For $X < 30$, it is also evident that impinging regions extend to the left side of the ribs. Comparing Fig. 8(a)–(c), the effects of rib-angle can be revealed. The performance of 60° rib arrangement seems only to be similar to that of 90° one. But, relatively, the 45° ribs result in a very strong heat transfer enhancement over the whole assembly of base plate and ribs. It is believed that the favorable vortical flow structure stemming from the appropriate sweep angle of the ribs is the major reason. From the Nu-contours on the rib top surface in Fig. 8(c), appearance

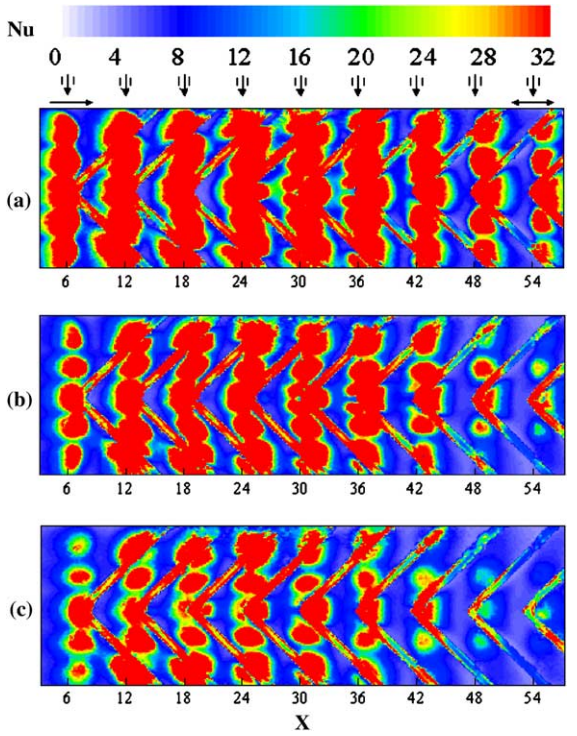

Fig. 7. Effects of jet-to-plate spacing on the on local heat transfer distributions for in-line jet array at $Re = 3000$, flow orientation 2, rib angle of 45° and jet-to-plate spacing Z of (a) 3; (b) 6 and (c) 9.

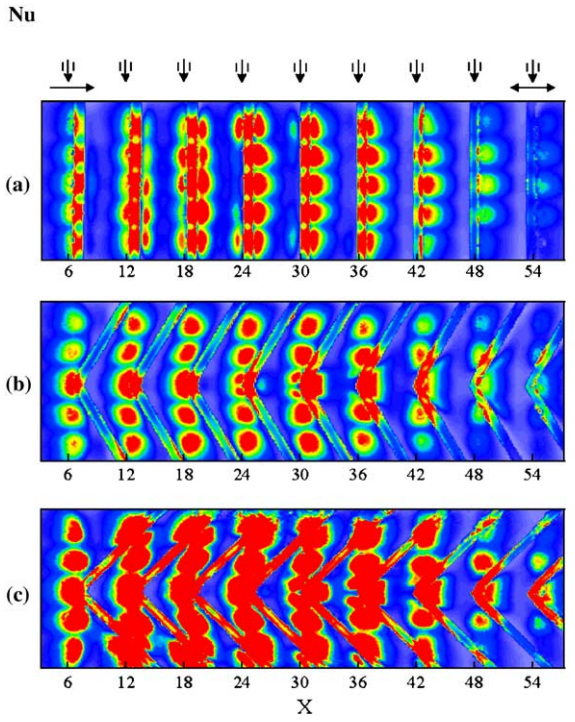

Fig. 8. Effects of rib angle on local heat transfer distributions for in-line jet array at $Re = 3000$, $Z = 6$, flow orientation 2 and rib angle of (a) 90°; (b) 60° and (c) 45°.

Table 1
Effects of jet-to-plate spacing Z on the averaged Nusselt number $\overline{Nu}$ of jet impingement on smooth or ribbed wall for $Re = 3000$ and flow orientation 2

	Jet arrangement	Smooth wall	45° Ribbed wall
$Z = 3$	In-line	36.99	64.94
	Staggered	33.41	55.48
$Z = 6$	In-line	29.12	37.62
	Staggered	19.12	26.36
$Z = 9$	In-line	5.72	26.31
	Staggered	6.43	20.71

Table 2
Effects of flow orientation and rib arrangement on the averaged Nusselt number $\overline{Nu}$ of in-line jet impingement on smooth or ribbed wall for $Re = 3000$ and $Z = 6$

	Smooth wall	90° Ribbed wall	60° Ribbed wall	45° Ribbed wall
Flow orientation 1	11.97	13.95	11.33	17.10
Flow orientation 2	29.12	16.71	15.95	37.62
Flow orientation 3	11.08	9.66	8.72	12.78

of swept vortical flows along the ribs can be inferred, and the vortices enhance the heat exchange between fluids and the solid boundaries. For numerical comparison of the effects of the rib arrangement on the jet impingement on the smooth or ribbed wall, Table 2 shows the averaged Nusselt number for different conditions. It is clearly observed in Table 2 that for the conditions of in-line jet arrangement, $Re = 3000$ and $Z = 6$, the heat transfer on the 60° and 90° ribbed walls is smaller than that on the smooth wall. But for the 45° rib arrangement, the heat transfer is better than that on the smooth wall.

With the arrangement of staggered array in Fig. 9(a)–(c), the general rules are similar as those of the in-line jet array. It is very interesting to note that for ribs of 90° and 60°, the staggered and in-line jet arrays have no remarkable difference in heat transfer performance. For ribs of 45°, however, the in-line jet array has better heat transfer characteristics than the staggered array. From the Nu-contours on the rib top surface in Fig. 8(c) and Fig. 9(c), appearance of swept vortical flows along the rib can be inferred, and the vortices augment

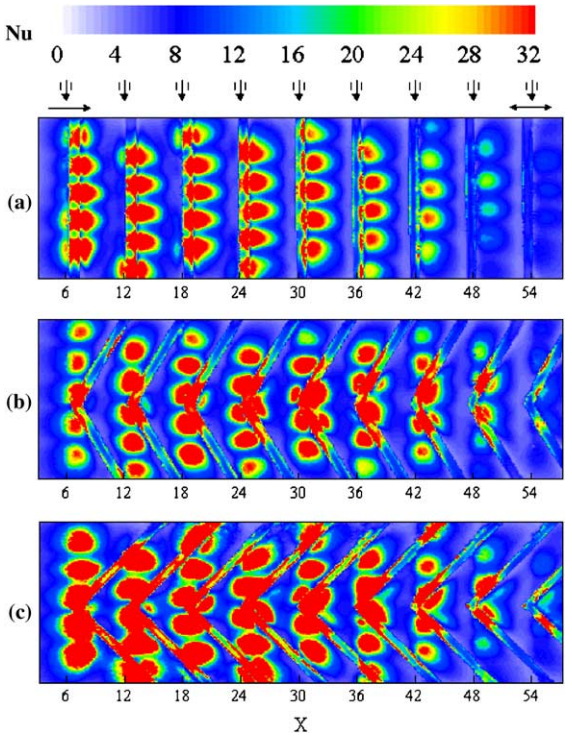

Fig. 9. Effects of rib angle on local heat transfer distributions for staggered jet array at $Re = 3000$, $Z = 6$, flow orientation 2 and rib angle of (a) 90°; (b) 60° and (c) 45°.

the heat transfer between fluids and the solid boundaries.

5. Conclusion

The local heat transfer rates on a target plate with angled ribs impinged by in-line or staggered jet array have been measured by using a transient liquid crystal technique. The present work concentrates on the effects of the exit flow orientation, rib arrangement and jet Reynolds number. It is found that the cross flow effect is closely related to the flow length experienced by the fluids after impingement. In the case of single exit, the upstream fluid travels a length near the length of the channel. For the two-exit cases, however, the fluids diverted to the both ends of the impingement channel. The short length of the development retains high transport rates in the thermal flow. With the presence of ribs, the heat transfer may be enhanced or retarded. As to the rib-angle effects, the best heat transfer enhancement are that stemming from a cascade of 45° V-type ribs placed evenly on the plate surface, by which favorable vortices can be generated with the sweep effect of the ribs.

Acknowledgement

The financial support of this study by the National Science Council of Taiwan, ROC, through the grant number NSC 90-2212-E211-008, is gratefully acknowledged.

References

[1] A.M. Huber, R. Viskanta, Effects of jet–jet spacing on convective heat transfer to confined, impinging arrays of axisymmetric air jets, Int. J. Heat Mass Transfer 37 (1994) 2859–2869.
[2] K. Garrett, B.W. Webb, The effect of drainage configuration on heat transfer under an impinging liquid jet array, ASME J. Heat Transfer 121 (1999) 803–810.
[3] L.W. Florschuetz, C.P. Truman, D.E. Metzger, Streamwise flow and heat transfer distribution for jet impingement with crossflow, ASME J. Heat Transfer 103 (1981) 337–342.
[4] V.J.H. Lienhard, Liquid jet impingement, in: C.L. Tien (Ed.), Annual Review of Heat Transfer, 6, Begell House, New York, 1995, pp. 199–270.
[5] V. Treuren, K.W. Wang, Z. Ireland, T.V. Jones, Detailed measurements of local heat transfer coefficient and adiabatic wall temperature beneath an array of impingement jets, ASME J. Turbomach. 116 (1994) 369–374.
[6] Y. Huang, S.V. Ekkad, J.C. Han, Detailed heat transfer distributions under an array of orthogonal impinging jets, AIAA J. Thermophys. Heat Transfer 12 (1998) 73–79.
[7] G.S. Azad, Y. Huang, J.C. Han, Impingement heat transfer on dimpled surfaces using a transient liquid crystal technique, AIAA J. Thermophys. Heat Transfer 14 (2) (2000) 186–193.
[8] W.M. Yan, R.C. Hsieh, C.Y. Soong, Experimental study of surface-mounted obstacle effects on heat transfer enhancement by using transient liquid crystal thermography, ASME J. Heat Transfer 124 (2002) 762–769.
[9] C. Gau, C.M. Chung, Surface curvature effect on slot-air-jet impingement cooling flow and heat transfer process, ASME J. Heat Transfer 113 (1991) 858–864.
[10] C. Gau, C.C. Lee, Impingement cooling flow structure and heat transfer along rib-roughened walls, Int. J. Heat Mass Transfer 35 (1992) 3000–3020.
[11] J.C. Han, Heat transfer and friction in channels with two opposite rib-roughened walls, ASME J. Heat Transfer 106 (1984) 774–781.
[12] J.C. Han, J.S. Park, C.K. Lei, Heat transfer enhancement in channels with turbulence promoters, ASME J. Eng. Gas Turb. Power 107 (1985) 628–635.
[13] J.C. Han, P.R. Chandra, S.C. Lau, Local heat/mass transfer distributions around sharp 180° turns in two-pass smooth and rib-roughened channels, ASME J. Heat Transfer 110 (1988) 91–98.
[14] S.C. Lau, R.D. McMillin, J.C. Han, Heat transfer characteristics of turbulent flow in a square channel with angled discrete ribs, ASME J. Turbomach. 113 (1991) 367–374.

[15] J.C. Han, Y.M. Zhang, High performance heat transfer ducts with parallel broken and V-shaped broken ribs, Int. J. Heat Mass Transfer 35 (1992) 513–523.
[16] W.M. Yan, H.C. Liu, C.Y. Soong, W.J. Yang, Experimental study of impingement heat transfer of incline and staggered jet arrays by using transient liquid crystal technique, J. Flow Visual. Image Process. 10 (2003) 119–141.
[17] W.M. Yan, H.S. Mei, H.C. Liu, C.Y. Soong, W.J. Yang, Measurement of detailed heat transfer on a surface under arrays of impinging elliptic jets by a transient liquid crystal technique, Int. J. Heat Mass Transfer 47 (2004) 5235–5245.